Journal of Inclusion Phenomena and Macrocyclic Chemistry (2024) 104:395–405
https://doi.org/10.1007/s10847-024-01240-6

ORIGINAL ARTICLE

Kinetics and thermodynamics of β-cyclodextrin-NH_2/β-carotene complexation: how much energy is required to include a hydrophobic group in the macrocycle cavity?

Yara Luiza Coelho[1,2,3] · Hauster Maximiler Campos de Paula[1] · Lívia Neves Santa Rosa[4] · Isabela Araujo Marques[1] · Nícolas Glanzmann[3] · Camilla Fonseca Silva[5] · Adilson David da Silva[3] · Clebio Soares Nascimento Jr.[5] · Ana Clarissa dos Santos Pires[4] · Luis Henrique Mendes da Silva[1]

Received: 16 November 2023 / Accepted: 11 March 2024 / Published online: 3 May 2024

Abstract

To improve the efficiency of cyclodextrins as carotenoid carriers, the kinetics and thermodynamics of the inclusion complex formation between modified β-cyclodextrin (βCD-NH_2) and β-carotene (βCT) were studied using surface plasmon resonance (SPR) at pH 7.4 and theoretical calculations. The observed dissociation rate of the [βCD-NH_2/βCT]° inclusion complex is small ($2.59 \times 10^{-1} s^{-1}$), indicating that βCD-$NH_2$ only interacted with the βCT ionone group to form inclusion complex. The βCD-NH_2/βCT binding constant is $2.80 \times 10^4 Lmol^{-1}$ (at 298.15 *K*), and its temperature dependence indicates that the [βCD-NH_2/βCT]° formation is driven by hydrophobic interactions ($\Delta H° = 28.83 kJmol^{-1}$ and $T\Delta S° = 54.21 kJmol^{-1}$) caused mainly by the βCT end group desolvation. In contrast, the formation of the [βCD-NH_2/βCT]‡ activated complex via association between free molecules and dissociation of [βCD-NH_2/βCT]° occurred with the overcoming of an energy barrier ($E_a^‡ = 40.77$ kJ mol^{-1} and $E_d^‡ = 11.94 kJmol^{-1}$) and decrease in entropy ($T\Delta S_a^‡ = -11.70 kJmol^{-1}$ and $T\Delta S_d^‡ = -65.92 kJmol^{-1}$).

Keywords β-carotene · β-cyclodextrin · Inclusion complex · Kinetic · Surface plasmon resonance · Thermodynamic

✉ Ana Clarissa dos Santos Pires
ana.pires@ufv.br

✉ Luis Henrique Mendes da Silva
luhen@ufv.br

Yara Luiza Coelho
yara.coelho@unifal-mg.edu.br

1 Advanced Thermokinetics of Molecular Systems (ATOMS) Group, Department of Chemistry, Federal University of Viçosa, PH Rolfs, Viçosa, MG 36570900, Brazil

2 Colloid Chemistry Group, Institute of Chemistry, Federal University of Alfenas, Gabriel Monteiro da Silva 700, Alfenas, MG 37130000, Brazil

3 Department of Chemistry, Institute of Exact Sciences, Federal University of Juiz de Fora, Juiz de Fora, MG 36036900, Brazil

4 Applied Molecular Thermodynamics, Department of Food Technology, Federal University of Viçosa, PH Rolfs, Viçosa, MG 36570900, Brazil

5 Applied Computational Chemistry Research Group, Department of Natural Sciences, Federal University of São João Del Rei, Dom Helvécio 74, Dom Bosco Campus, São João Del Rei, MG 36301160, Brazil

Introduction

Despite the progress made in food and pharmaceutical industries in the 21st century, complications due to vitamin A deficiency still cause blindness and even deaths worldwide [1]. Therefore, vitamin A supplementation programs and food and beverage fortification technologies are of relevance for combating malnutrition in low-income and middle-income countries, which are the ones that struggle the most with this problem [2].

β-carotene (βCT) is a precursor of vitamin A and an antioxidant with various potential benefits such as vision protection, anti-cancer agent, and reducing sunburn [3, 4]. Given these benefits and the growing demands for organic foods, the use of βCT as a bio-functional ingredient in food matrices has become an important innovation in the food and pharmaceutical industries. However, the incorporation of βCT into food products has proven to be a major technological challenge [5] as its polyene chain structure and ionone end groups cause it to have poor water solubility and make it vulnerable to modification by environmental

factors such as temperature, pH, and light. Consequently, it has low bioavailability, which severely restricts its use and application [5, 6].

Many studies have sought to improve the stability and solubility of bioactive molecules through structural modification or the use of additives [7–9]. However, these methods are both complex and inefficient. In this context, molecular inclusion has emerged as an effective method that can be used to stabilize and improve the solubility and bioavailability of βCT. Furthermore, studies have shown that β-cyclodextrin (βCD) is a potential candidate for the stabilization and subsequent inclusion of bioactive molecules [10–12].

βCD is a cyclic oligosaccharide composed of seven units of glucopyranose. It has a truncated cone shape with the capacity to enclose (partially or fully) small bioactive molecules. The ability of this compound to form inclusion complexes (ICs) is due to its hydrophobic cavity and hydrophilic exterior, in which its cavity and exterior simultaneously interact with the guest (generally containing hydrophobic segments) and solvent molecules, respectively [13]. Thus, properties such as solubility, stability, volatility, and controlled release of bioactive molecules can be modulated using this complexing agent [14]. Other benefits of using βCD in the food industry are its lower cost, compared to α- and γ-cyclodextrin, and non-toxicity, as it is considered a Generally Recognized as Safe molecule by the United States Food and Drug Administration [15, 16].

In recent years, the use of βCD as a complexing agent for bioactive molecules has become the focus of many studies [17–19]. Specifically, the formation of βCD/βCT ICs and their structure and properties (stoichiometry, water-solubility, resistance to oxidation, as well as emulsification and antioxidant capacities) have been investigated using spectroscopic (nuclear magnetic resonance (NMR), UV–Vis, Raman, Fourier transform infrared spectroscopy (FTIR)) and microscopic methods [20–22]. Polyakov et al. studied the interaction between β-caroten-8'-oic acid and βCD via ^{1}H-NMR and UV–Vis measurements and found direct evidence for the formation of a 1:1 IC and the improvement of the carotenoid's chemical stability [21]. Additionally, using Raman spectroscopy and quantum mechanics calculations, Oliveira et al. found that the structure of the IC consists of βCD near the extremities (ionone group) of the βCT molecules. Furthermore, the molecules assumed a more extended conformation after the inclusion process [22]. Nevertheless, the fundamental aspects that are associated with the kinetics and thermodynamics of complexation between these species need to be further elucidated. Until today, the velocity of formation and dissociation of the ICs formed by the interaction between βCD and βCT as well as their thermodynamic stability or the driving forces that drive their formation remain unclear, which limit the applicability of these nano-aggregates in food and pharmaceutical systems. Understanding the energetics and dynamics of complexation between these species will allow the determination of the optimal conditions for applying the system, thereby improving the bioavailability of βCT.

By recognizing this gap in knowledge and the importance of these fundamental studies in the development of new technologies for delivering carotenoids, here, the surface plasmon resonance (SPR) technique was used to provide the kinetic and thermodynamic information regarding the inclusion process of βCD/βCT. The SPR technique makes it possible to determine the energetics and molecular dynamics associated with the formation of βCD/βCT ICs in a single experiment. In this way, it is possible to understand and modulate the molecular processes responsible for the formation of these supramolecular structures, allowing to fully explore their scientific and technological potential [23, 24].

The immobilization of the host molecule in the SPR chip surface was possible through the functionalization of the βCD with an amine group (βCD-NH_2) which was then used for all experiments. The association (k_a) and dissociation (k_d) kinetic rate constants as well as the activation (activation energy ($E^{\ddagger}$), variations in Gibbs free energy ($\Delta G^{\ddagger}$), enthalpy ($\Delta H^{\ddagger}$) and entropy ($T\Delta S^{\ddagger}$) of activation), and thermodynamic (equilibrium binding constant (K_b), standard Gibbs free energy change ($\Delta G°$), standard enthalpy change ($\Delta H°$), and standard entropy change ($\Delta S°$)) parameters were obtained to understand and propose an inclusion mechanism for the complex formed.

Materials and methods

Materials

βCD (≥ 97%wt.), βCT (≥ 93%wt., Fig. 1), analytical-grade sodium acetate, dimethyl sulfoxide (DMSO), iodine, triphenylphosphine, imidazole, and ethylenediamine were purchased from Sigma-Aldrich (St. Louis, MO, USA). βCDs functionalized with an amine group (mono-(6-ethanediamine-6-deoxy)-β-cyclodextrin), as shown in Fig. 1, were synthesized according to the method described by Hudson et al. (2022) with a yield of 85%. ^{1}H NMR (500 MHz, D_2O) δ 5.05 (d, 7 H, J = 3.7 Hz), 3.93 (t, 7 H, J = 9.5 Hz), 3.89–3.81 (m, 21 H), 3.63 (dd, 7 H, J = 9.5, 3.7 Hz), 3.57 (t, 7 H, J = 9.5 Hz), 3.22 (t, 2 H, J = 5.8 Hz), 2.93 (t, 2 H, J = 5.8 Hz).

CM5 sensor chips, *N*-ethyl-*N*'-(dimethylaminopropyl) carbodiimide (EDC), *N*-hydroxysuccinimide (NHS), ethanolamine hydrochloride, and HBS-P running buffer (0.01 M HEPES, 0.15 M NaCl, and 0.005%v/v surfactant P20 at pH 7.4) were acquired from GE Healthcare (Pittsburgh, PA, USA). All the materials were used without further

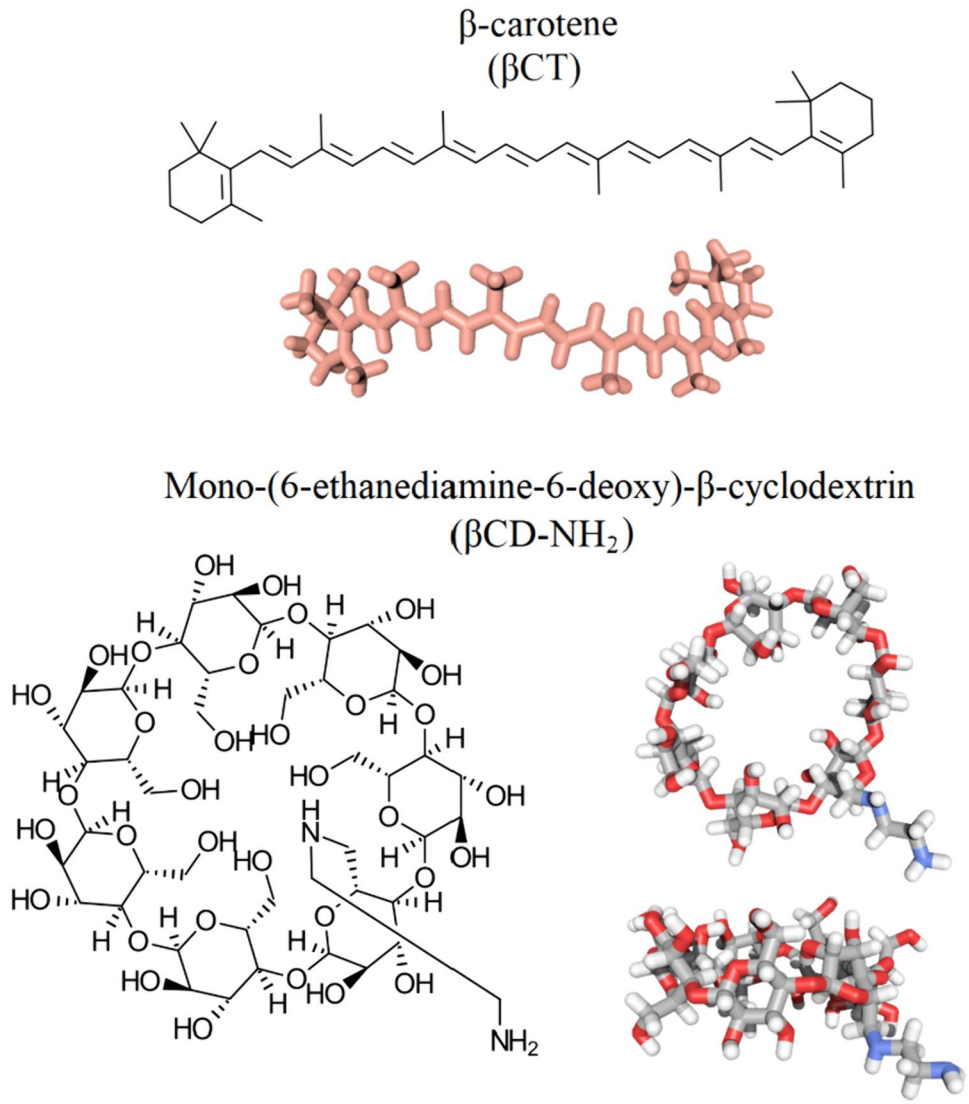

Fig. 1 Chemical structures of βCT and βCD-NH_2 immobilized on SPR sensor chip surface

purification and the solutions were prepared using deionized water obtained from a Milli-Q system (Millipore, Burlington, MA, USA).

Methods

SPR measurements

SPR measurements were conducted in triplicates using a two-channel Biacore® X100 device (GE Healthcare, Pittsburgh, PA, USA). The measurements involve the following steps: immobilization of βCD-NH_2 on the chip surface and analysis of the βCT interactions with the immobilized βCD-NH_2. The procedures were described in detail in the following sections.

Immobilization of βCD-NH_2 on the chip surface The immobilization of βCD-NH_2 on the surface of the CM5 sensor chip was performed using the standard covalent amine coupling method (Fig. 2) [25]. Following the insertion of the CM5 sensor chip into Biacore® X100, its carboxyl groups were first activated using a mixture of EDC (0.4 M) and NHS (0.1 M) solution (1:1 v/v) at a flow rate of 10 μL min^{-1} for 7 min. Then, a solution of 2.6×10^{-5} M βCD-NH_2, which was prepared in 10 mM sodium acetate (pH 4.0), was injected at a flow rate of 10 μL min^{-1} for 7 min, resulting in low-density βCD-NH_2 immobilization (1200 RU) that minimized the potential mass transport and agglomeration. Finally, excess activated carboxyl groups were blocked with ethanolamine for 7 min. To monitor possible non-specific interactions between the oligosaccharides and chip surface, a reference channel was prepared as described above but without the βCD-NH_2 immobilization.

Kinetic and thermodynamic analyses of β-carotene inclusion on immobilized βCD-NH_2 The formation of ICs between

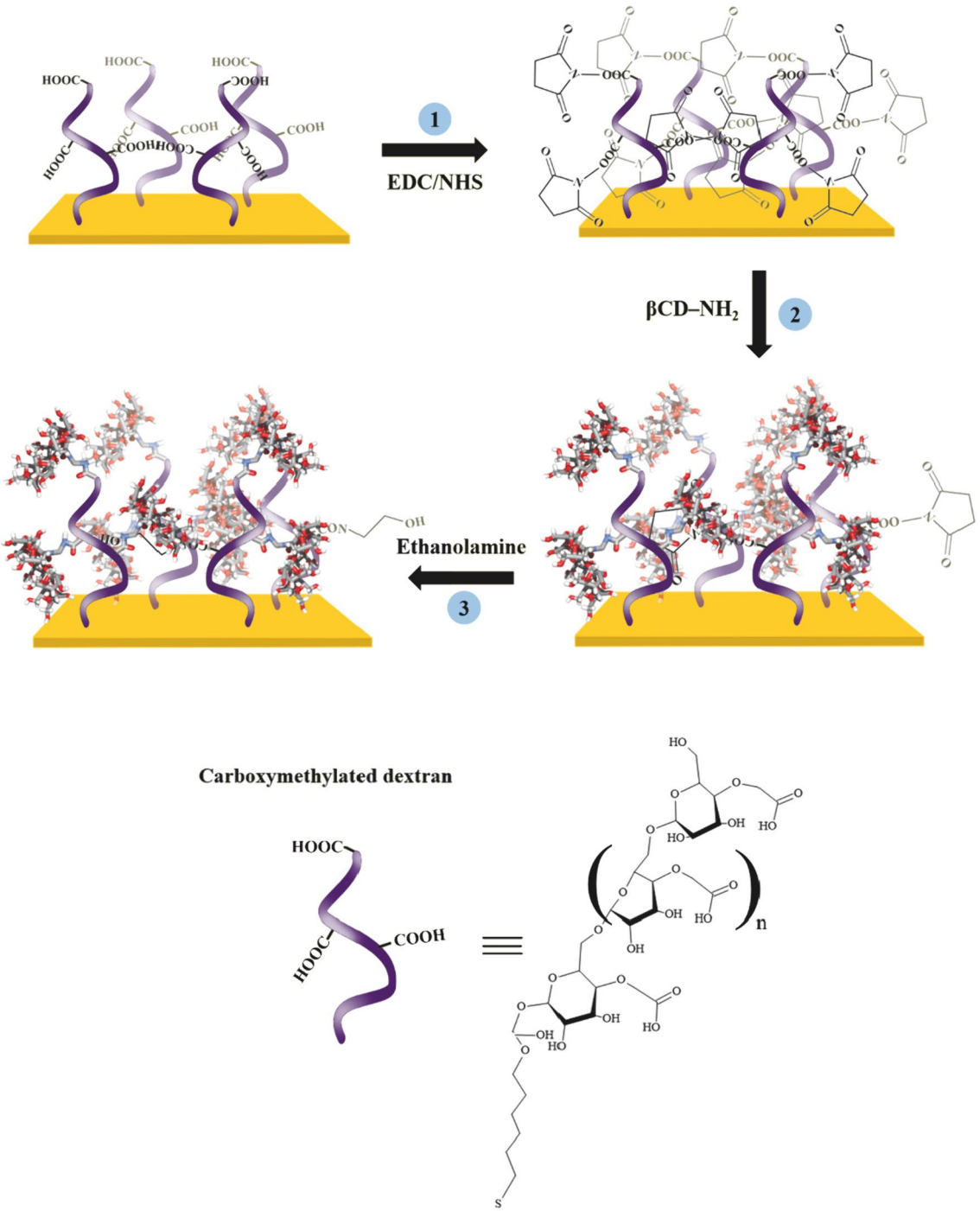

Fig. 2 Immobilization of βCD-NH_2 on the CM5 chip surface. (1) Activation of the carboxyl groups of the carboxymethylated dextran using a mixture of EDC and NHS; (2) Low-density immobilization of βCD-NH_2 (1200 RU); and (3) Block of excess activated carboxyl groups with ethanolamine

βCD-NH_2 and βCT were analyzed at pH 7.4 and six different temperatures (285.15–301.15 K). βCT solutions, with concentrations ranging from 10 to 35 µM, were prepared in HBS-P buffer (0.01 M HEPES pH 7.4, 0.15 M NaCl, and 0.005%v/v surfactant P20) and DMSO (4%v/v). The buffer was injected prior to each βCD-NH_2/βCT interaction cycle to obtain the baseline. Then, βCT solutions of various concentrations were injected over both the sample and reference channels of the sensor chip for 12 s at a flow rate of 10 µL min^{-1}. Subsequently, the pure buffer was injected twice for 30 s into both

chip channels at a flow rate of 10 µL min^{-1} to dissociate the formed ICs and regenerate the chip surface at the end of each experiment. Subtraction of the reference and sample channel signals was performed, and the net SPR signals (in resonance units, RU) were traced over time (sensorgrams). To ensure accuracy, all SPR experiments were performed in triplicates.

Kinetics to determine the kinetics of the βCD-NH_2/βCT inclusion process, the integrated rate equations (Eqs. 1 and 2) were globally fitted to the sensorgram date (Fig. S1), and the observed (k_{obs}) and dissociation (k_d) kinetic constants were calculated as follows [26]:

$$\mathrm{RU}(t) = \mathrm{RU}_{\max(t_\infty)}\left[1 - e^{-k_{obs}(t-t_0)}\right], \tag{1}$$

$$\mathrm{RU}(t) = \mathrm{RU}(t_m)e^{-k_d(t-t_m)}, \tag{2}$$

where RU(t) is the SPR response at time t, $\mathrm{RU}_{\max(t_\infty)}$ is the SPR response in the βCD-NH_2 saturation condition by βCT, and $\mathrm{RU}(t_m)$is the SPR signal at the time when only the buffer flows over the CM5 sensor chip.

The k_{obs} value was used to determine the association rate constant (k_a) value from the slope of k_{obs} versus [βCT] (Eq. 3, Fig. S2).

$$k_{obs} = k_a[\beta\mathrm{CT}] + k_d \tag{3}$$

The temperature dependence of ln$k_a$and lnk_d can be analyzed using the linear Arrhenius approach (Eq. 4, Fig. S3) to determine the activation energy ($E_x^{\ddagger}$) required to form the [βCD-NH_2/βCT]‡ activated complex via the association of free βCT with immobilized βCD-NH_2 ($E_a^{\ddagger}$) or the dissociation of the thermodynamically stable [βCD-NH_2/βCT]° complex ($E_d^{\ddagger}$), respectively.

$$E_x^{\ddagger}(T) = -R\left(\frac{d\ln k_x}{d1/T}\right), \tag{4}$$

where k_x is the association (x = a) or dissociation (x = d) rate constant, $E_x^{\ddagger}$is the activation energy, R is the universal gas constant (8.314 J mol^{-1} K), and T is the temperature (in K).

According to transition state theory, the change in activation Gibbs free energy ($\Delta G_x^{\ddagger}$) can be calculated using Eq. 5. Additionally, the changes in activation enthalpy ($\Delta H_x^{\ddagger}$) and activation entropy ($T\Delta S_x^{\ddagger}$) can be obtained using Eqs. 6 and 7, respectively [27].

$$\Delta G_x^{\ddagger}(T) = -RTln\left(\frac{k_x h}{K_B T}\right), \tag{5}$$

$$\Delta H_x^{\ddagger}(T) = E_x^{\ddagger}(T) - RT, \tag{6}$$

$$T\Delta S_x^{\ddagger}(T) = \Delta H_x^{\ddagger}(T) - \Delta S_x^{\ddagger}(T), \tag{7}$$

where K_B and h are the Boltzmann and Planck constants, respectively.

Thermodynamics the $K_b$value associated with the [βCD-NH_2/βCT]° formation can be obtained by calculating the ratio between the kinetic rate constants [28], as expressed in Eq. 8.

$$K_b = \frac{k_a}{k_d} \tag{8}$$

Furthermore, $\Delta G°$ was calculated from the K_b values (Eq. 9). Additionally, ΔH^o and ($T\Delta S^{\circ}$) were obtained using the linear van't Hoff approach (Eq. 10, Fig. S4) and fundamental Gibbs relation (Eq. 11), respectively [29].

$$\Delta G^{\circ} = -RT\ln K_b \tag{9}$$

$$\ln\left(\frac{K_b(T_2)}{K_b(T_1)}\right) = -\frac{\Delta H^{\circ}}{R}\left(\frac{1}{T_2} - \frac{1}{T_1}\right) \tag{10}$$

$$\Delta G^{\circ} = \Delta H^{\circ} - T\Delta S^{\circ} \tag{11}$$

Statistics

The standard deviations of the measured and calculated parameters were obtained, respectively, from the regression of the experimental data and by following the rules of propagation of uncertainty.

Theoretical details

A sequential theoretical methodology based on PM3 semiempirical and Density Functional Theory (DFT) calculations, employing the B97D functional with the Pople's split valence 6-311G (d,p) basis set containing polarization functions on all atoms, was performed to fully optimize the inclusion complex formed between the βCD-NH_2 and βCT. The 1:1 complex stoichiometry was assumed based on previous experimental findings [30].

The initial guess geometry for the βCD-NH_2/βCT inclusion complex was fully optimized at the semiempirical PM3 level of theory. PM3 harmonic frequency calculations were also performed for the equilibrium structure, characterizing it as true minimum on the potential energy surface (all frequencies were real). Posteriorly, the electronic energy contribution was estimated by single point B97D/6-31G(d,p)// PM3 calculations using the fully optimized PM3 geometries. This so-called sequential methodology has been successfully used for cyclodextrins supramolecular complexes [31].

All theoretical calculations were performed on Gaussian 09 quantum mechanical package [32].

Results and discussion

Formation of IC between βCD-NH_2 and βCT

The SPR technique is widely used to determine the kinetic parameters, binding affinities, and specificity of real-time and label-free bimolecular interactions [33]. Therefore, to confirm and elucidate the formation of βCD-NH_2/βCT ICs, as well as their molecular dynamics and energy of interaction, sensorgrams of immobilized βCD-NH_2 interacting with βCT were recorded at different temperatures, as shown in Fig. 3 and S1.

The flow of the βCT solution over the βCD-NH_2 surface resulted in sensorgram profiles that were typical of bimolecular interactions. When a pure buffer flows on the CM5 surface, the same SPR signal is observed in the reference and sample channels, producing an RU signal in the sensorgram that equals zero (baseline). Immediately after injecting the βCT solution into both SPR channels, a continuous increase in the RU signal was observed over time, which demonstrates the interaction between βCT and βCD-NH_2. This increase in the SPR signal was due to the simultaneous processes of association of the free molecules and dissociation of the thermodynamically stable complex [βCD-NH_2/βCT]°, with the predominance of the association process. When $t \rightarrow \infty$, metastable equilibrium is reached, in which the speed of association is equal to that of dissociation (sensorgram plateau). After this plateau, the flow of βCT was interrupted, and only the buffer returned to flow over the chip, which resulted in the dissociation of the complexes formed and a gradual decrease in the RU values until it reached the baseline value. The complete sensorgram demonstrated that the interaction between βCT and βCD-NH_2 was fully reversible under the physiological conditions. Confirmation of the βCD-NH_2/βCT reversible interaction is a crucial factor for the future use of these nano-aggregates in the encapsulation, transport, and controlled release of these bioactive molecules in living organisms [11].

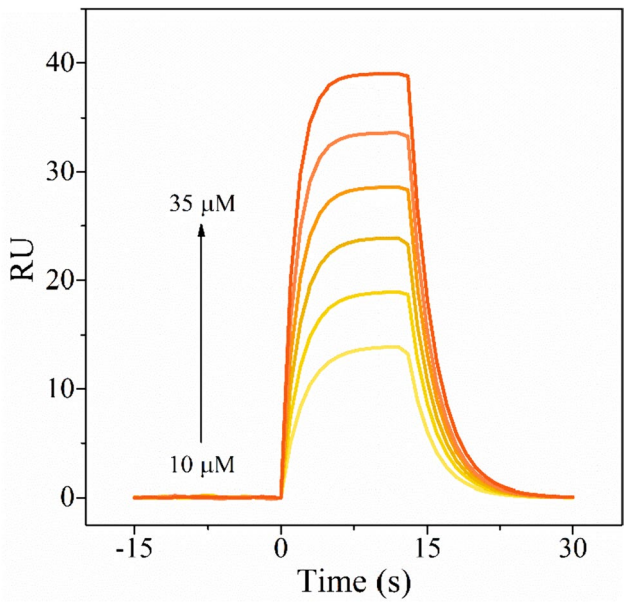

Fig. 3 Sensograms of immobilized βCD-NH_2 interacting with βCT in the range of 10 to 35 μM at pH 7.4 and 298.15 K

Polyakov et al. demonstrated that βCD formed 1:1 ICs with βCT [21]. Therefore, to better understand the dynamics and energetics of the molecular recognition mechanisms that lead to the formation of these ICs, the kinetics and thermodynamics of the βCD-NH_2/βCT interaction were determined and are discussed in the following sections.

Kinetics of βCD-NH_2/βCT complexation

The kinetic rate constants obtained using the SPR analysis provide essential information on the velocity of IC formation and dissociation. The knowledge serves as the foundation for the application of these complexes as nano-carriers [34].

Based on a previous study [20, 21] and the sensorgrams obtained from this study, the interaction between βCD-NH_2 and βCT can be described by a simple reversible biomolecular mechanism of binding for the formation of 1:1 IC (Eq. 12).

$$\beta\text{CD}-\text{NH}_2 + \beta\text{CT} \underset{k_d}{\overset{k_a}{\rightleftharpoons}} \left[\beta\text{CD}-\text{NH}_2/\beta\text{CT}\right]^{\circ} \tag{12}$$

The time required for βCT to associate with βCD-NH_2 is reflected by k_a, whereas the lifetime of the [βCD-NH_2/βCT]° complexes is governed by k_d. Using the k_d values, we can obtain the residence time ($\tau_R = 1/k_d$), i.e., the lifetime of the guests in the βCD-NH_2 cavity, which may be directly related to the efficiency of delivery and chemical protection of the bioactive compounds. Therefore, to obtain the kinetic rate constants, a 1:1 Langmuir interaction model (Eqs. 1, 2, 3) was applied to the sensorgram data, and the values of k_a, k_d, and τ_R at different temperatures are listed in Table 1.

The values of k_a and k_d increase with increasing temperature, demonstrating that the increase in the average molecular kinetic energy increased the association rate between βCD-NH_2 and βCT free molecule and the dissociation rate of [βCD-NH_2/βCT]° complex. The τ_R values range from 3.26 to 2.5 s, indicating that the exchange time between the complexes and free species was similar to the inclusion process of other bioactive molecules [25].

Table 1 k_a, k_d, and τ_R values for the interaction between βCD-NH_2 and βCT (pH 7.4) at different temperatures

T	k_a	k_d	τ_R
K	10^3 $M^{-1}s^{-1}$	10^{-1} s^{-1}	s
285.15	5.0	3.07	3.26
289.15	6.5	3.31	3.02
293.15	7.8	3.56	2.81
297.15	10.0	3.78	2.64
298.15	10.8	3.86	2.59
301.15	12.5	4.00	2.50

For all parameters, the standard deviation is less than 4%

To understand the molecular dynamics of IC formation between βCD-NH_2 and bioactive molecules, it is essential to characterize the energetics involved in the formation of the activated complex, the intermediate species that are formed before the free molecules become the thermodynamically stable complex [35]. Therefore, it would be of interest to determine the energetic parameters of activation that are associated with the formation of [βCD-NH_2/βCT]‡ activated complex, including the association process of βCD-NH_2 and βCT free molecules ($x = a$) and the dissociation process of [βCD-NH_2/βCT]° ($x = d$), that is, the activation energy ($E_x^‡$) and changes in Gibbs free energy ($\Delta G_x^‡$), enthalpy ($\Delta H_x^‡$), and entropy ($T\Delta S_x^‡$) of activation.

The rate constants obtained at different temperatures (Table 1) were used to calculate the $E_x^‡$ values (Eq. 4) using an Arrhenius plot ($\ln k_a$ or $\ln k_d$ versus 1/T, Fig. S3). From the $E_x^‡$ values, $\Delta H_x^‡$ for the [βCD-NH_2/βCT]‡ formation were calculated using Eq. 6, whereas $\Delta G_x^‡$ and $\Delta S_x^‡$ were obtained using Eqs. 5 and 7, respectively. The values of these parameters are listed in Table 2.

The $\Delta G_a^‡$ and $\Delta G_d^‡$ values were positive and predominantly remained constant with increasing temperature; however, the Gibbs free energy barrier for the [βCD-NH_2/βCT]‡ formation from the [βCD-NH_2/βCT]° dissociation was higher than that of the association of free βCT and βCD-NH_2 molecules.

The $\Delta G_x^‡$ values can be expressed as the results of different molecular processes to the [βCD-NH_2/βCT]‡ formation [36]:

$$\Delta G_x^‡ = \Delta G_{x-conf}^‡ + \Delta G_{x-int}^‡ + \Delta G_{x-des}^‡, \quad (13)$$

where $\Delta G_{x-conf}^‡$ accounts for possible conformational changes in βCT and βCD-NH_2 that are necessary for the formation of [βCD-NH_2/βCT]‡, $\Delta G_{x-int}^‡$, reflects the direct βCD-NH_2/βCT interaction, and $\Delta G_{x-des}^‡$ is the contribution of H_2O molecules that are released from the cavity of βCD-NH_2 to the bulk solution ($\Delta G_{x-des/\beta CD}^‡$) and the desolvation of βCT molecules ($\Delta G_{x-des/\beta CT}^‡$). Since $\Delta G_x^‡$ results from the contributions of the potential energy barrier ($E_x^‡$ or $\Delta H_x^‡$), and configurational and conformational entropy change barriers ($T\Delta S_x^‡$), to better analyze the difference between $\Delta G_a^‡$ and $\Delta G_d^‡$ values one could rationalize $E_x^‡$, $\Delta H_x^‡$ and $T\Delta S_x^‡$ in terms of these same molecular processes.

$E_a^‡$ and $\Delta H_a^‡$ represent the energy barriers for the penetration of βCT into the βCD-NH_2 cavity. Here, the values obtained were positive and temperature-independent, suggesting that [βCD-NH_2/βCT]‡ was formed in a single step. The magnitude of these energetic parameters is primarily due to the energy required to break the solvation layer of βCT ($E_{a-des/\beta CT}^‡$ and $\Delta H_{a-des/\beta CT}^‡ > 0$), which overcomes the energy released from the desolvation of the βCD cavity ($E_{a-des/\beta CD}^‡$ and $\Delta H_{a-des/\beta CD}^‡ < 0$) [37], changes in the conformation of both host and guest molecules ($E_{a-conf}^‡$ and $\Delta H_{a-conf}^‡ < 0$), and the formation of new βCD-NH_2/βCT interactions to form [βCD-NH_2/βCT]‡ ($E_{a-int}^‡$ and $\Delta H_{a-int}^‡ < 0$). The predominance of the βCT desolvation process on the $E_a^‡$ and $\Delta H_a^‡$ values was probably associated with the high hydrophobicity of the ionone group encapsulated by the βCD-NH_2 cavity. This is a plausible hypothesis upon the comparison of our results with those obtained by Hudson et al., in which they studied the inclusion of RES ($\Delta H_a^‡ = 12.33$ kJ mol^{-1}) and RESAn1 ($\Delta H_a^‡ = 57.96$ kJ mol^{-1}) in βCD-NH_2 and found that the $E_a^‡$ and $\Delta H_a^‡$ values

Table 2 Energetic parameters of activation for the formation of [βCD-NH_2/βCT]‡ via association between immobilized βCT and βCD-NH_2 free molecules as well as for the dissociation of [βCD-NH_2/βCT]° at pH 7.4

T	Association phase (*a*)				Dissociation phase (*d*)			
	$E_a^‡$	$\Delta H_a^‡$	$\Delta G_a^‡$	$T\Delta S_a^‡$	$E_a^‡$	$\Delta H_d^‡$	$\Delta G_d^‡$	$T\Delta S_d^‡$
K	kJ mol^{-1}							
285.15	40.77	38.40	49.54	− 11.13	11.94	9.57	72.53	− 62.96
289.15		38.37	49.63	− 11.27		9.53	73.40	− 63.86
293.15		38.33	49.91	− 11.57		9.50	74.27	− 64.77
297.15		38.30	50.01	− 11.71		9.47	75.17	− 65.70
298.15		38.29	50.00	− 11.70		9.46	75.38	− 65.92
301.15		38.27	50.16	− 11.89		9.44	76.07	− 66.64

For all parameters, the standard deviation is less than 4%

were also positive and followed the molecules' order of hydrophobicity (RES < βCT < RESAn1) [25].

On the other hand, $T\Delta S_a^{\ddagger}$ values were negative but also remained almost constant over the investigated temperature range. The formation of $[\beta CD-NH_2/\beta CT]^{\ddagger}$ from the association of βCT and βCD-NH_2 free molecules occurs with partial loss of translational and rotational degrees of freedom upon interaction ($T\Delta S_{a-int}^{\ddagger} < 0$), as well as, negative entropy contribution resulting from a rather straight conformation assumed by βCT ($T\Delta S_{a-conf}^{\ddagger} < 0$) and desolvation of the βCD cavity ($T\Delta S_{a-des/\beta CD}^{\ddagger} < 0$). However, the small $T\Delta S_a^{\ddagger}$ negative values (compared to $T\Delta S_d^{\ddagger}$) indicate that the entropically favorable dehydration process of the βCT hydrophobic moiety ($T\Delta S_{a-des/\beta CT}^{\ddagger} > 0$) also contributes to the formation of the activated complex.

Although the energetic parameters for the dissociation of $[\beta CD-NH_2/\beta CT]^{\circ}$ to form $[\beta CD-NH_2/\beta CT]^{\ddagger}$ were higher than those for the association, their values were temperature-independent and occurred with positive values of $E_d^{\ddagger}$ and $\Delta H_d^{\ddagger}$ and negative values of $T\Delta S_d^{\ddagger}$. Unlike the association process, the roto-translational degrees of freedom and solvation layers of the molecules probably do not change during the dissociation process because in both thermodynamically stable and activated complexes, the βCT molecule is already encapsulated inside the βCD-NH_2 cavity. Therefore, the $E_d^{\ddagger}$, $\Delta H_d^{\ddagger}$, and $T\Delta S_d^{\ddagger}$ values obtained indicate that more energy is absorbed to break the interactions in $[\beta CD-NH_2/\beta CT]^{\circ}$ than released from the formation of new ones in $[\beta CD-NH_2/\beta CT]^{\ddagger}$, which results in a simultaneous structuring of the βCD-NH_2 cavity and the βCT terminal group, thereby reducing the entropy.

Based on this kinetic analysis, the βCD-NH_2/βCT inclusion mechanism can be thought to comprise the following steps (Fig. 4): (i) βCT approaches the immobilized βCD-NH_2 and adopts an appropriate orientation; (ii) some of the solvating water molecules are released from the βCT ionone group and βCD-NH_2 cavity. βCT is partially encapsulated inside the cavity via the secondary hydroxy rim, which is the more open side of the conical cyclodextrin. (iii) After the cavity inclusion, a conformational fit occurs, in which the orientations of the guest and host molecules become more restricted, with the βCT structure adopting a more extended conformation. It is at this step that $[\beta CD-NH_2/\beta CT]^{\ddagger}$ is reached; and (iv) with deeper penetration of the guest molecule, stronger intermolecular interactions are formed with βCD-NH_2 and βCT can finally adopt a more relaxed conformation to form $[\beta CD-NH_2/\beta CT]^{\circ}$.

Thermodynamics of βCD-NH_2/βCT complexation

Complementary to kinetic parameters, thermodynamic analysis is also useful for understanding the molecular recognition mechanism between the host and guest molecules. The SPR systems not only allow the investigation of kinetics but also the thermodynamics and specificity of the IC molecular interactions [25, 38]. To the best of our knowledge, there are no thermodynamic data in the literature on the inclusion of βCT in βCD. Therefore, to gain further insight into the stability and driving forces for the $[\beta CD-NH_2/\beta CT]^{\circ}$ formation, the values of K_b (Eq. 8), ΔG° (Eq. 9), ΔH° (Eq. 10), and $T\Delta S^{\circ}$ (Eq. 11) were also calculated from the SPR data and are listed in Table 3.

Table 3 K_b, ΔG°, ΔH°, and $T\Delta S^{\circ}$ values for the thermodynamically stable complexes of $[\beta CD-NH_2/\beta CT]^{\circ}$ at different temperatures and pH 7.4

T K	K_b $10^4\ M^{-1}$	ΔH°	ΔG° kJ mol^{-1}	$T\Delta S^{\circ}$
285.15	1.63	28.83	− 22.99	51.82
289.15	1.96		− 23.76	52.60
293.15	2.19		− 24.36	53.19
297.15	2.65		− 25.16	53.99
298.15	2.80		− 25.38	54.21
301.15	3.13		− 25.91	54.75

For all parameters, the standard deviation is less than 4%

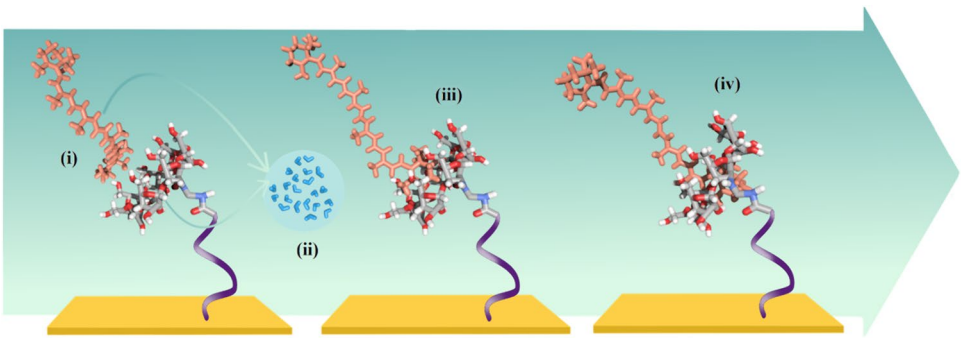

Fig. 4 Schematic of the proposed inclusion mechanism between βCD-NH_2 and βCT

In all the temperatures studied, the $K_b$values were in the order of 10^4 M^{-1}, which resulted in the negative values of $\Delta G°$, indicating that the complexation between βCT and βCD-NH_2 is favored in thermodynamic equilibrium. To determine the driving forces for the formation of these complexes, the enthalpic and entropic contributions were analyzed.

The positive $\Delta H°$ and $T\Delta S°$ values indicated that hydrophobic forces dominated the formation of [βCD-NH_2/βCT]°. Therefore, although there are other processes occurring in this system that lead to a decrease in enthalpy and entropy (e.g., desolvation of the βCD-NH_2 cavity, conformational changes, and formation of the βCD-NH_2/βCT pair), they are overcame by contributions coming from desolvating the highly hydrophobic ionone moiety of the βCT molecule. In this process, highly structured H_2O molecules in the solvation shell of these groups are released into the solution bulk, resulting in an increase in the enthalpy and entropy of the system.

Although there are no studies on the thermodynamics of βCT inclusion by βCD-NH_2, Qiao et al. recently investigated the interaction between a modified carotenoid, i.e., astaxanthin behenic acid monoester (Asta-C22:0), and hydroxypropyl–βCD (HPβCD) via phase solubility analyses [39]. They found that the inclusion of Asta-C22:0 occurred in the ionone group, which is similar to that of βCT. However, unlike in our study, the IC formation was enthalpically driven ($\Delta H°$ = −26.95 kJ mol^{-1} and $T\Delta S°$ = 0.31 kJ mol^{-1}), owing to the fact that the included portion of Asta-C22:0 is a derivative of the ionone group that contains a hydroxyl group, making it less hydrophobic.

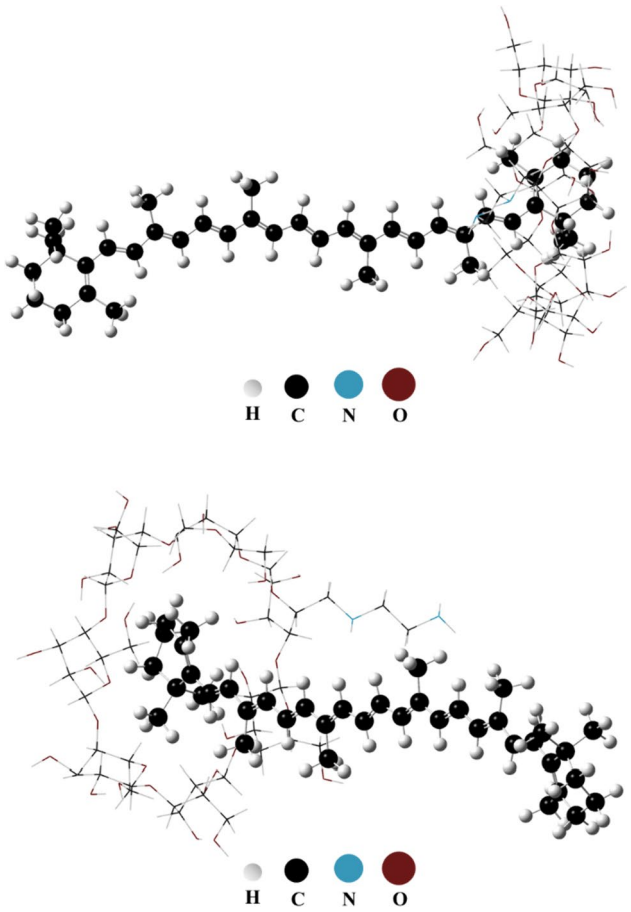

Fig. 5 PM3 fully optimized geometry of the βCD-NH_2/βCT ICs in two views

Theoretical results

The electronic complexation energy (ΔE = − 71.5 kJ mol^{-1}) and Gibbs free energy (ΔG = − 24 kJ mol^{-1}), were obtained via B97D/6-31G(d,p)//PM3 calculations for the βCD-NH_2/βCT complex, whose optimized geometry is shown in Fig. 5.

According to these results, the inclusion complex formation is spontaneous and favored in the thermodynamic equilibrium, besides the driving forces responsible for stabilizing the guest in the host cavity are mostly the weak ones, such as London dispersion forces. These results are in accordance with the ones obtained experimentally by SPR, and confirms that the IC formed consists of the ionone group of βCT encapsulated by the βCD-NH_2.

Conclusions

SPR assay was used to analyze the kinetics and thermodynamics of the inclusion process of the βCD-NH_2/βCT complex. The presence of hydrophobic groups at the end of the guest molecules induces the formation of thermodynamically stable [βCD-NH_2/βCT]° IC that was dominated by hydrophobic forces, as corroborated by theoretical calculations. The inclusion of βCT in the βCD-NH_2 cavity first occurred with the formation of an intermediate state, [βCD-NH_2/βCT]‡. To reach this intermediate state, the molecules had to surpass the energetic ($\Delta H_a^{‡}$ = 38.29kJmol^{-1})and entropic $T\Delta S_a^{‡}$ = −11.70kJmol^{-1}) barriers that originated mainly from the desolvation of the ionone group and the conformation changes of βCT, respectively. Next, deeper penetration of βCT in the βCD-NH_2 cavity occurs with the restructuring of the pair (formation of new interactions), resulting in the formation of the thermodynamically stable [βCD-NH_2/βCT]° IC. Because the inclusion is a dynamic process, [βCD-NH_2/βCT]° also dissociates into [βCD-NH_2/βCT]‡ with unfavorable enthalpy ($\Delta H_d^{‡}$ = 9.46kJmol^{-1}) and entropy ($T\Delta S_d^{‡}$ = −65.92kJmol^{-1}) changes of the system. The thermodynamic data showed that [βCD-NH_2/βCT]° was stable at all studied temperatures ($K_b \cong 10^4$ and

$\Delta G° = -25.38 kJmol^{-1}$) and its formation was entropy-driven ($\Delta H° = 28.83 kJmol^{-1}$ and $T\Delta S° = 54.21 kJmol^{-1}$). Our results contribute to fundamental knowledge that can aid future applications of βCD/carotenoid ICs to enhance the solubility and stability of these bioactive molecules in food matrices.

Supplementary material

Figures showing the sensograms (RU × time) for the interaction kinetics of 10–35 µM βCT with βCD-NH_2 at different temperatures (Fig. S1); plot of k_{obs} as a function of βCT concentration for the determination of k_a at different temperatures (Fig. S2); Arrhenius plots of ln k_a and ln k_a versus 1/T that are associated with the formation of the βCD-NH_2/βCT IC (Fig. S3); plot of ln k_a versus $1/T$ (van't Hoff approach) for the inclusion of βCT in βCD-NH_2 (Fig. S4).

Supplementary Information The online version contains supplementary material available at https://doi.org/10.1007/s10847-024-01240-6.

Acknowledgements Y. L. C thanks the CNPq (151136/2020-3) for post-doctoral fellowship.

Author contributions Yara Luiza Coelho: conceptualization, methodology, investigation, writing—original draft; Hauster Maximiler Campos de Paula: investigation and formal analysis; Lívia Neves Santa Rosa: investigation and editing; Isabela Araujo Marques: formal analysis and writing—review; Nícolas Glanzmann: formal analysis, resources, writing—review and editing; Camilla Fonseca Silva: formal analysis, writing—review; Adilson David da Silva: supervision, funding acquisition, writing—review and editing; Clebio Soares Nascimento Jr.: supervision, writing—review and editing; Ana Clarissa dos Santos Pires: supervision, funding acquisition, writing—review and editing; Luis Henrique Mendes da Silva: conceptualization, writing— original draft, supervision, project administration, funding acquisition.

Funding This work was supported by the *Conselho Nacional de Desenvolvimento Científico e Tecnológico* (CNPq), *Coordenação de Aperfeiçoamento de Pessoal de Nível Superior* (CAPES), and *Fundação de Amparo à Pesquisa do Estado de Minas Gerais* (FAPEMIG).

Data availability No datasets were generated or analysed during the current study.

Declarations

Conflict of interest The authors declare that they have no known competing financial interests or personal relationships that could have appeared to influence the work reported in this paper.

References

1. Khanna, P.: Food based strategies to combat micronutrient malnutrition. Int. J. Food Sci. Nutr. Int. **2**, 37–39 (2018)
2. Stevens, G.A., Bennett, J.E., Hennocq, Q., Lu, Y., De-Regil, L.M., Rogers, L., Danaei, G., Li, G., White, R.A., Flaxman, S.R., Oehrle, S.P., Finucane, M.M., Guerrero, R., Bhutta, Z.A., Then-Paulino, A., Fawzi, W., Black, R.E., Ezzati, M.: Trends and mortality effects of vitamin A deficiency in children in 138 low-income and middle-income countries between 1991 and 2013: a pooled analysis of population-based surveys. Lancet Glob Health **3**, e528–e536 (2015). https://doi.org/10.1016/S2214-109X(15)00039-X
3. Kawata, A., Murakami, Y., Suzuki, S., Fujisawa, S.: Anti-inflammatory activity of β-carotene, lycopene and tri-n-butylborane, a scavenger of reactive oxygen species. Vivo (Brooklyn). **32**, 255–264 (2018). https://doi.org/10.21873/invivo.11232
4. Eggersdorfer, M., Wyss, A.: Carotenoids in human nutrition and health. Arch. Biochem. Biophys. **652**, 18–26 (2018). https://doi.org/10.1016/j.abb.2018.06.001
5. Boon, C.S., McClements, D.J., Weiss, J., Decker, E.A.: Factors influencing the chemical stability of carotenoids in foods. Crit. Rev. Food Sci. Nutr. **50**, 515–532 (2010). https://doi.org/10.1080/10408390802565889
6. Gul, K., Tak, A., Singh, A.K., Singh, P., Yousuf, B., Wani, A.A.: Chemistry, encapsulation, and health benefits of β-carotene—a review. Cogent Food Agric. **1**, 1018696 (2015). https://doi.org/10.1080/23311932.2015.1018696
7. Rezaei, A., Fathi, M., Mahdi, S.: Nanoencapsulation of hydrophobic and low-soluble food bioactive compounds within di ff erent nanocarriers. Food Hydrocoll. **88**, 146–162 (2019). https://doi.org/10.1016/j.foodhyd.2018.10.003
8. Chung, C., Rojanasasithara, T., Mutilangi, W., McClements, D.J.: Stabilization of natural colors and nutraceuticals: inhibition of anthocyanin degradation in model beverages using polyphenols. Food Chem. **212**, 596–603 (2016). https://doi.org/10.1016/j.foodchem.2016.06.025
9. Pertig, D., Schäfer, C., Ulrich, J.: Stabilization of carotenoids. Chem. Eng. Technol. **35**, 1045–1050 (2012). https://doi.org/10.1002/ceat.201200052
10. Pinho, E., Grootveld, M., Soares, G., Henriques, M.: Cyclodextrins as encapsulation agents for plant bioactive compounds. Carbohydr. Polym. **101**, 121–135 (2014). https://doi.org/10.1016/j.carbpol.2013.08.078
11. Soukoulis, C., Bohn, T.: A comprehensive overview on the micro- and nano-technological encapsulation advances for enhancing the chemical stability and bioavailability of carotenoids. Crit. Rev. Food Sci. Nutr. **58**, 1–36 (2018). https://doi.org/10.1080/10408398.2014.971353
12. Liu, Y., Chen, Y., Gao, X., Fu, J., Hu, L.: Application of cyclodextrin in food industry. Crit. Rev. Food Sci. Nutr. **1**, 1–15 (2020). https://doi.org/10.1080/10408398.2020.1856035
13. Mura, P.: Analytical techniques for characterization of cyclodextrin complexes in aqueous solution: a review. J. Pharm. Biomed. Anal. **101**, 238–250 (2014). https://doi.org/10.1016/j.jpba.2014.02.022
14. Del, E.M.M., Valle: Cyclodextrins and their uses: a review. Process Biochem. **39**, 1033–1046 (2004). https://doi.org/10.1016/S0032-9592(03)00258-9
15. Astray, G., Gonzalez-Barreiro, C., Mejuto, J.C., Rial-Otero, R., Simal-Gándara, J.: A review on the use of cyclodextrins in foods. Food Hydrocoll. **23**, 1631–1640 (2009). https://doi.org/10.1016/j.foodhyd.2009.01.001
16. Ozkan, G., Franco, P., De Marco, I., Xiao, J., Capanoglu, E.: A review of microencapsulation methods for food antioxidants: principles, advantages, drawbacks and applications. Food Chem. **272**, 494–506 (2019). https://doi.org/10.1016/j.foodchem.2018.07.205
17. Zhao, M., Wang, H., Yang, B., Tao, H.: Identification of cyclodextrin inclusion complex of chlorogenic acid and its antimicrobial activity. Food Chem. **120**, 1138–1142 (2010). https://doi.org/10.1016/j.foodchem.2009.11.044

18. Wang, J., Cao, Y., Sun, B., Wang, C.: Physicochemical and release characterisation of garlic oil-β-cyclodextrin inclusion complexes. Food Chem. **127**, 1680–1685 (2011). https://doi.org/10.1016/j.foodchem.2011.02.036
19. Krishnaswamy, K., Orsat, V., Thangavel, K.: Synthesis and characterization of nano-encapsulated catechin by molecular inclusion with beta-cyclodextrin. J. Food Eng. **111**, 255–264 (2012). https://doi.org/10.1016/j.jfoodeng.2012.02.024
20. Yildiz, Z.I., Topuz, F., Kilic, M.E., Durgun, E., Uyar, T.: Encapsulation of antioxidant beta-carotene by cyclodextrin complex electrospun nanofibers: solubilization and stabilization of beta-carotene by cyclodextrins. Food Chem. **423**, 136284 (2023). https://doi.org/10.1016/j.foodchem.2023.136284
21. Polyakov, N.E., Leshina, T.V., Konovalova, T.A., Hand, E.O., Kispert, L.D.: Inclusion complexes of carotenoids with cyclodextrins: 1HNMR, EPR, and optical studies. Free Radic Biol. Med. **36**, 872–880 (2004). https://doi.org/10.1016/j.freeradbiomed.2003.12.009
22. de Oliveira, V.E., Almeida, E.W.C., Castro, H.V., Edwards, H.G.M., Dos Santos, H.F.: De Oliveira, carotenoids and β-cyclodextrin inclusion complexes: Raman spectroscopy and theoretical investigation. J. Phys. Chem. A. **115**, 8511–8519 (2011). https://doi.org/10.1021/jp2028142
23. Singh, V., He, Y., Wang, C., Xu, J., Xu, X., Li, H., Singh, P., York, P., Sun, L., Zhang, J.: A comparison report of three advanced methods for drug-cyclodextrin interaction measurements. J. Pharm. Biomed. Anal. **134**, 252–258 (2017). https://doi.org/10.1016/j.jpba.2016.11.037
24. Wu, D., Wu, W., Tang, L., Hu, X., Zhang, J., Li, H., Li, H.: Simulation-guided relationships and interaction characteristics of human CtBP1 in complex with protocatechualdehyde. J. Mol. Liq (2022). https://doi.org/10.1016/j.molliq.2022.119507
25. Hudson, E.A., de Paula, H.M.C., Coelho, Y.L., Glanzmann, N., da Silva, A.D., da Silva, L.H.M., Pires, A.C.: The kinetics of formation of resveratrol-β-cyclodextrin-NH2 and resveratrol analog-β-cyclodextrin-NH2 supramolecular complexes. Food Chem. **366**, 1–8 (2022). https://doi.org/10.1016/j.foodchem.2021.130612
26. Rezende, J.P., Hudson, E.A., de Paula, H.M.C., Meinel, R.S., da Silva, A.D., dos Pires, A.C., Da Silva, L.H.M.: Human serum albumin-resveratrol complex formation: effect of the phenolic chemical structure on the kinetic and thermodynamic parameters of the interactions. Food Chem. **307**, 125514 (2020). https://doi.org/10.1016/j.foodchem.2019.125514
27. Petersson, G.A.: Perspective on the activated complex in chemical reactions. Theor. Chem. Acc. **103**, 190–195 (2000). https://doi.org/10.1007/s002149900102
28. Mohammadzadeh-Asl, S., Aghanejad, A., Yekta, R., de la Guardia, M., Ezzati Nazhad Dolatabadi, J., Keshtkar, A.: Kinetic and thermodynamic insights into interaction of erlotinib with epidermal growth factor receptor: surface plasmon resonance and molecular docking approaches. Int. J. Biol. Macromol. **163**, 954–958 (2020). https://doi.org/10.1016/j.ijbiomac.2020.07.048
29. de Castro, A.S.B., de Paula, H.M.C., Coelho, Y.L., Hudson, E.A., Pires, A.C.S., Da Silva, L.H.M.: Kinetic and thermodynamic of lactoferrin—ethoxylated-nonionic surfactants supramolecular complex formation. Int. J. Biol. Macromol. **187**, 325–331 (2021). https://doi.org/10.1016/j.ijbiomac.2021.07.087
30. Kaur, M., Bawa, M., Singh, M.: β–carotene-β–cyclodextrin inclusion complex: towards. J. Global Biosiences **5**, 3665–3675 (2016)
31. de Sousa, F.B., Leite Denadai, Â.M., Lula, I.S., Nascimento, C.S., Fernandes Neto, N.S.G., Lima, A.C., de Almeida, W.B., Sinisterra, R.D.: Supramolecular self-assembly of cyclodextrin and higher water soluble guest: thermodynamics and topological studies. J. Am. Chem. Soc. **130**, 8426–8436 (2008). https://doi.org/10.1021/ja801080v
32. Frisch, M.J., Trucks, G., Schlegel, H.B., Scuseria, G.E., Robb, M.A., Cheeseman, J., Scalmani, G., Barone, V., Mennucci, B., Petersson, G.A., Nakatsuji, H., Caricato, M., Li, X., Hratchian, H.P., Izmaylov, A.F., Bloino, J., Zheng, G., Sonnenberg, J., Hada, M., Fox, D.: Uranyl extraction by N, N-dialkylamide ligands studied by static and dynamic DFT simulations. Gaussia **9**, 227 (2009)
33. Ravindran, N., Kumar, S., Yashini, M., Rajeshwari, S., Mamathi, C.A., Nirmal Thirunavookarasu, S., Sunil, C.K.: Recent advances in surface plasmon resonance (SPR) biosensors for food analysis: a review. Crit. Rev. Food Sci. Nutr. **1**, 1–23 (2021). https://doi.org/10.1080/10408398.2021.1958745
34. Kobayashi, H., Endo, T., Ogawa, N., Nagase, H., Iwata, M., Ueda, H.: Evaluation of the interaction between B-cyclodextrin and psychotropic drugs by surface plasmon resonance assay with a Biacore® system. J. Pharm. Biomed. Anal. **54**, 258–263 (2011). https://doi.org/10.1016/j.jpba.2010.08.012
35. EYEING, H.: The activated complex and the absolute rate of chemical reactions. Chem. Rev. **17**, 65–77 (1935)
36. Chen, W., Chang, C.-E., Gilson, M.K.: Calculation of cyclodextrin binding affinities: energy, entropy, and implications for drug design. Biophys. J. **87**, 3035–3049 (2004). https://doi.org/10.1529/biophysj.104.049494
37. Agudelo, Á.J.P., Coelho, Y.L., Ferreira, G.M.D., Ferreira, G.M.D., Hudson, E.A., dos Pires, A.C., Da Silva, L.H.M.: Solvophobic effect of 1-alkyl-3-methylimidazolium chloride on the thermodynamic of complexation between β-cyclodextrin and dodecylpyridinium cation. Colloids Surf. Physicochem Eng. Asp **582**, 123850 (2019). https://doi.org/10.1016/j.colsurfa.2019.123850
38. Magalhães, O.F., De Paula, H.M.C., de Rezende, J., Coelho, Y.L., de Mendes, T.A., Da Silva, L.H.M., dos Pires, A.C.: Energetic and molecular dynamic characterization of lysozyme/β-carotene interaction. J. Mol. Liq. **337**, 1–10 (2021). https://doi.org/10.1016/j.molliq.2021.116404
39. Qiao, X., Yang, L., Hu, X., Cao, Y., Li, Z., Xu, J., Xue, C.: Characterization and evaluation of inclusion complexes between astaxanthin esters with different molecular structures and hydroxypropyl-β-cyclodextrin. Food Hydrocoll. **110**, 106208 (2021). https://doi.org/10.1016/j.foodhyd.2020.106208